Electronic Supplementary Material (ESI) for Energy & Environmental Science.

Electronic Supplementary Information

Perovskite promoted iron oxide for hybrid water-splitting and syngas generation with exceptional conversion

Feng He, and Fanxing Li*[a]

Department of Chemical and Biomolecular Engineering, North Carolina State University, 911 Partners Way, Raleigh, NC 27695-7905, USA.
**Email: Fli5@ncsu.edu*

This Supplementary information contains the following sections:

Experimental method

Redox Catalyst Synthesis

Lanthanum strontium ferrite ($La_{0.8}Sr_{0.2}FeO_{3-\delta}$ or LSF) supported Fe_3O_4 is used as the redox catalyst. We reported that LSF being an effective, mixed ionic-electronic conductive support to inhibit sintering of iron/iron oxides, thereby enhancing the redox activity and thermal stability of iron oxide based redox catalysts.[1] Fe_3O_4-LSF (25wt% LSF), Fe_3O_4-LSF (40wt% LSF), and pure LSF are synthesized by a solid-state reaction (SSR) method: a stoichiometric amount of precursors, i.e. iron oxide (Fe_2O_3, 99.9%, Noah Chemicals), La_2O_3 (99.9%, Aldrich), and $SrCO_3$ (99.9%, Noah Chemical), are weighed. This is followed by ball-milling, pelletization, and sintering at 1200°C for 12 hours. The resulting pellets are subsequently crushed and sieved into 75 to 150 μm. A reference redox catalyst, i.e. Fe_3O_4-$MgAl_2O_4$ (40wt% $MgAl_2O_4$), is prepared with an identical method. Since the as-prepared redox catalysts are composed of Fe_2O_3 and LSF support, one cycle reduction followed with steam regeneration is performed to obtain Fe_3O_4 phase. Crystallite phases of the resulting redox catalysts are confirmed using X-ray powder diffraction (XRD) (Rigaku SmartLab).

Fixed bed experiment

Redox experiments are carried out in a stainless steel tubular reactor with an inner diameter of 5 mm (Figure S1) under a fixed-bed mode. The reactor is externally heated with a tube furnace (MTI OTF-1200X-S-VT**)** with K type thermocouple measuring the temperature. A gas mixing panel with multiple Brooks mass flow controllers (MFCs) is used to deliver gaseous mixtures, e.g. nitrogen and methane, to the reactor. In each experiment, 2 to 3 grams of redox catalyst particles are added on top of the SiC layer which serves as a gas distributor. In order to mimic the hybrid redox scheme, the tests are carried out in two consecutive steps, i.e. methane partial oxidation (redox catalyst reduction) and water-splitting (redox catalyst oxidation). The redox reaction temperature is set at 930 °C. 15 ml min^{-1} (STP: standard temperature 0°C and pressure 1 atm) N_2 is used as the internal standard in both reduction and oxidation steps. 10 ml min^{-1} (STP) CH_4 is introduced along with N_2 from the top of the reactor. Water-splitting reaction is carried out after the residue gas from the methane oxidation step has been completely purged with N_2. In the oxidation step, water is injected by a syringe pump (NE-300 Just Infusion™) from the bottom of the reactor at a rate of 0.278 mmol min^{-1}. Prior to entering the reactor, the water is vaporized and preheated. Compositions of the gases exiting the reactor are determined using a gas chromatograph (Agilent Micro GC 490) and a multi-gas analyzer (Emerson X-Stream gas analyzer). Parameters for evaluating the redox experiments are summarized in Table S1, where $\dot{n}_i$ is the molar flow rate of component *i*, and in/out represents inlet/outlet steams of the reaction.

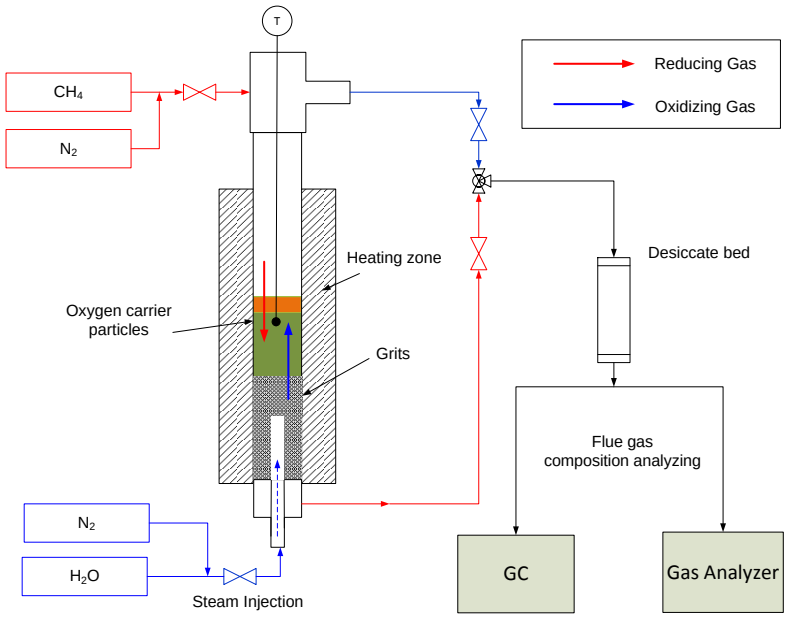

Figure S1: Experimental setup for hybrid redox process test with Fe_2O_3-LSF particle

Table S1: Summary of parameters used to characterize the redox reactions

Parameters	Equations
CH_4 Conversion	$(1-\frac{\dot{n}_{CH_4,out}}{\dot{n}_{CH_4,in}})\times 100\%$
Syngas yield	$\frac{\dot{n}_{H_2,out}+\dot{n}_{CO,out}}{3\dot{n}_{CH_4,in}}\times 100\%$
Steam to H_2 Conversion	$\frac{\dot{n}_{H_2,out}}{\dot{n}_{H_2O,in}}\times 100\%$
H_2 Purity	$\frac{\dot{n}_{H_2,out}}{\dot{n}_{H_2,out}+\dot{n}_{CO,out}+\dot{n}_{CO_2,out}}\times 100\%$

H_2 analysis

The concentration of H_2 in the experiment is determined by an online micro-GC (Agilent CP-490) with a molecular sieve 5A column. The GC is calibrated to achieve the correlation coefficient of R>0.998 for H_2. Flow rate of H_2 generated is calculated by

$$V_{H_2}=\int(X_{H_2}F_{Total})dt=\int(X_{H_2}\frac{F_{N_2}}{X_{N_2}})dt \qquad \text{Equation S1}$$

where F is the flow rate, X is the mole fraction and V is the total volume of the gas. N_2 is used as an internal standard. When CO and/or CO_2 is detected in the oxidation step, H_2 generated from carbon deposition is excluded based on the stoichiometry of steam carbon reactions:

$C + H_2O \leftrightarrow CO + H_2$ Reaction S1

$C + 2H_2O \leftrightarrow CO_2 + 2H_2$ Reaction S2

Steam to H_2 conversion is then calculated by the amount of H_2 generated divided by the injected H_2O. The flow rate of the syringe pump is independently calibrated through a gravimetric method. All the gas flows in the experiment are controlled by Brooks 5850E mass flow controllers (MFCs) which has 0.25% of rate in repeatability. Before each experiment, the gas flow rates are calibrated by a Bios Flow Calibrator (DryCal Definer 220 Primary) and a bubble flowmeter.

Steam Conversion Verification using a Thermal Gravimetric Analyzer (TGA)

Since steam conversion is an important parameter for the current study, a TGA (TA Instrument) with external reducing and oxidizing gas injection is used to independently verify steam conversion of the redox catalysts. A schematic of the TGA setup is shown in Figure S2. The aforementioned gas mixing panel with multiple mass flow controllers (MFCs) is used to deliver gaseous mixtures. The experiments are conducted with a sample weight of approximately 20 mg at a specific isothermal temperature. 200 ml min^{-1} N_2 and 50 ml min^{-1} H_2 is used as reducing gas, which is injected after the temperature reaches the setting. After 4 hours reduction or when the sample weight change is less than 0.01 mg ml min^{-1}, H_2 flow is stopped. This is followed with injection of oxidizing gas i.e. H_2 and steam mixture. To ensure accurate injection of steam, a gas mixture of N_2 and H_2 is injected into a bubbler at 50 °C to generate concentrated steam. The high concentration steam is then passed through another bubbler at 20 °C (5 ˚C below room temperature) to create a gaseous stream that contains 2.34 mol% steam prior to entering the TGA. The premixed H_2-steam allows for accurate verification of steam conversion. To determine the maximum steam conversion, H_2 flow rate is reduced by 1 ml min^{-1} until the sample weight in TGA start to increase. Provided that weight gain or oxidation of the redox catalyst is observed in the TGA at a given H_2 mole fraction X_{H2}, defined by $\frac{F(H_2)}{F(H_2)+F(H_2O)} \times 100\%$, the redox catalyst is concluded to be capable of achieving steam conversion higher than X_{H2}. The crystalline phases of the post-experiment redox catalysts are analyzed using X-ray powder diffraction (XRD) (Rigaku SmartLab) with Cu-Kα (λ=0.1542 nm) radiation within the 20-80° 2θ angle range.

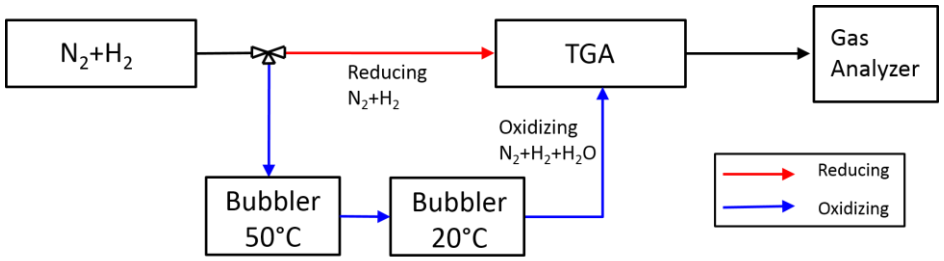

Figure S2: Schematic of TGA experimental setup with injection of reducing and oxidizing gases

Second law analysis on the impact of steam conversion on process efficiency

Figure S3 shows a simplified schematic for exergy analysis on the water-splitting reaction. *X* mole of H_2O is converted into 1 mol H_2, with the steam conversion of *1/X*. In order to obtain the minimum exergy loss, we optimistically assume that the sensible heat for water and steam preheating can be fully recovered from product cooling with no heat loss. The most irreversible step is then resided in the product condensation step. It is noted that the product stream would have a lower total pressure (P2) and steam mole fraction *(X-1)/X* than those in the feed stream. Therefore, steam partial pressure and hence dew point of the product is lower than those of the feedstock. As a result, latent heat from steam condensation in the product stream cannot be fully recoverable. In addition, a minimum temperature difference, typically >5 K, is required for effective heat exchange. This means that water-vaporization prior to water-splitting needs to be provided by external energy sources. If we further assume, optimistically, that a turbine is available to recover the latent heat from product steam condensation at 85% of Carnot efficiency with 40 ˚C discharge temperature,[2,3] the exergy loss can be calculated using the following equation:

$$\Delta b = b_2 - b_1 = (1-\frac{T_o}{T_1})X\Delta\hat{H}_{evp} + 0.85(1-\frac{313}{T_r})5X\hat{C}_{P,steam} - 0.85(1-\frac{313}{T_2})(X-1)\Delta\hat{H}_{evp} \quad \text{Equation S2}$$

For each additional mole of water being heated and condensed, the minimal exergy loss is estimated to be:

$$\Delta\hat{b} = (1-\frac{T_o}{T_1})\Delta\hat{H}_{evp} + 0.85(1-\frac{313}{T_r})5\hat{C}_{P,steam} - 0.85(1-\frac{313}{T_2})\Delta\hat{H}_{evp} \quad \text{Equation S3}$$

ΔH_{evp} is the mole heat of vaporization of water. T_o is the standard temperature of 298K and T_1 is steam boiling temperature of 398K at 1 atm. T_2 is the temperature at which latent heat from the unconverted steam is recovered (393K in this case). T_r is the temperature for the water-splitting reaction. Assuming a system pressure of 1 atm and water-splitting temperature of 1123K, minimum exergy loss is therefore estimated to be 3.05 kJ mol^{-1} of unconverted steam. Therefore, higher energy conversion efficiency can be anticipated with high steam to hydrogen conversion.

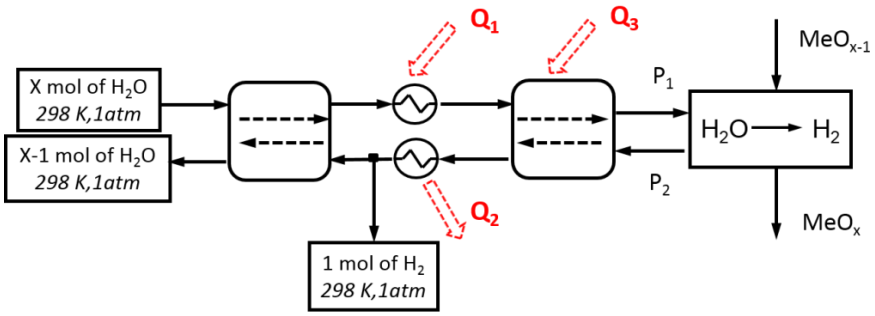

Figure S3: Exergy analysis on a simplified thermochemical water-splitting scheme

Steam conversion in the FeO_x-H_2O-H_2 ternary system under equilibrium conditions

Thermodynamic analysis can provide maximum steam to H_2 conversion in the steam-iron reactions under varying temperatures. When metallic iron is oxidized to wüstite, steam has the highest conversion as compared to steam reaction with other types of iron oxides, as shown in the equilibrium phase diagram for the FeO_x-H_2O-H_2 ternary system (Figure S4).[4] At the reaction temperature of interest, wüstite typically exhibits cation deficiency with formula of $FeO_{0.947}$. As a result, water-splitting reaction: $0.947Fe + H_2O = Fe_{0.947}O + H_2$ should have the highest steam conversion for the FeO_x-H_2O-H_2 ternary system. Steam conversion (X) can be calculated by the following equation:

$$K = e^{-\frac{\Delta G}{RT}} = \frac{p_{H_2}}{p_{H_2O}} = \frac{X}{1-X} \qquad \text{Equation S4}$$

where K is the equilibrium constant, ΔG is the free energy change of the reaction at the given temperature. Using HSC Chemistry v7, the thermodynamic steam conversion as a function of temperature is calculated and the results are shown in Table S2. Steam conversion decreases with increasing temperatures. At 930 °C, the steam to hydrogen equilibrium conversion is 62.3%. Such a conversion is confirmed using ASPEN Plus®.

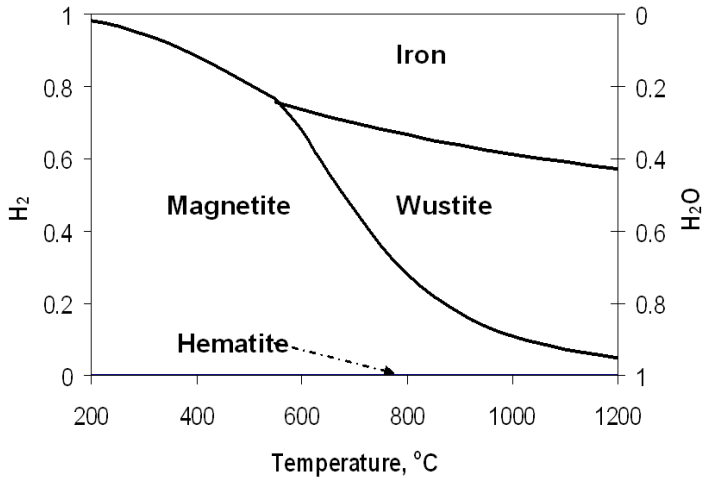

Figure S4: Phase diagram of the FeO_x-H_2O-H_2 ternary system

Table S2: Maximum steam to hydrogen conversion calculated by thermodynamic equilibrium

T	Steam Conversion
750 °C	68.8%
800 °C	66.8%
850 °C	65.0%
900 °C	63.3%
930 °C	62.3%
1000 °C	60.2%

Non-stoichiometry within $La_{0.8}Sr_{0.2}FeO_{3-\delta}$ perovskite

Perovskite used in the present work has a general formula of $La_{0.8}Sr_{0.2}FeO_{3-\delta}$ (LSF). The Sr acceptor doped perovskite exhibits varying degree of oxygen non-stiochiometry at different oxygen partial pressures. A defect model[5,6] proposed by Mizusaki et al. is used to calculate the oxygen nonstoichiometry δ. Based on the model, the reaction between O_2 and oxygen defects in $La_{1-x}Sr_xFe_{3-\delta}$ is expressed as

$$\frac{1}{2}O_2(g)+V_O^{\bullet\bullet}+Fe_{Fe}^{x}=O_O^{x}+2Fe_{Fe}^{\bullet} \qquad \text{Reaction S3}$$

The equilibrium constant K_{ox} is

$$K_{Ox}=\frac{\left[O_O^{\times}\right]\left[Fe_{Fe}^{\bullet}\right]^2}{p_{o_2}^{\frac{1}{2}}\left[V_O^{\bullet\bullet}\right]\left[Fe_{Fe}^{\times}\right]^2}=\frac{(3-\delta)\left[Fe_{Fe}^{\bullet}\right]^2}{p_{o_2}^{\frac{1}{2}}\delta\left[Fe_{Fe}^{\times}\right]^2} \qquad \text{Equation S5}$$

$$p_{O_2}^{\frac{1}{2}}=K_{wat}\frac{p_{H_2O}}{p_{H_2}} \qquad \text{Equation S6}$$

The concentration of iron with different charges is determined by disproportionation of Fe^{III} to Fe^{II} and Fe^{IV}:

$$2Fe_{Fe}^{\times}=Fe_{Fe}^{\bullet}+Fe_{Fe}^{'} \qquad \text{Reaction S3}$$

The equilibrium constant K_{Fe} is

$$K_{Fe}=\frac{\left[Fe_{Fe}^{\bullet}\right]\left[Fe_{Fe}^{'}\right]}{\left[Fe_{Fe}^{\times}\right]^2} \qquad \text{Equation S7}$$

For $La_{0.8}Sr_{0.2}FeO_{3-\delta}$

$$\left[Fe_{Fe}^{\times}\right]+\left[Fe_{Fe}^{\bullet}\right]+\left[Fe_{Fe}^{'}\right]=1 \qquad \text{Equation S8}$$

$$x+\left[Fe_{Fe}^{'}\right]=2\delta+\left[Fe_{Fe}^{\bullet}\right] \qquad \text{Equation S9}$$

Combined Equations S5 to S9,

$$\frac{\delta^{\frac{1}{2}}(2\delta-x+1)}{(3-\delta)^{\frac{1}{2}}(2\delta-x)}K_{wat}^{\frac{1}{2}}p_{o_2}^{\frac{1}{4}}=\frac{K_{Fe}}{K_{Ox}}\frac{(1+x-2\delta)(3-\delta)^{\frac{1}{2}}}{\delta^{\frac{1}{2}}(2\delta-x)}\frac{1}{K_{wat}^{\frac{1}{2}}p_{o_2}^{\frac{1}{4}}}-\frac{1}{K_{Ox}^{\frac{1}{2}}} \qquad \text{Equation S10}$$

where x = 0.2 for $La_{0.8}Sr_{0.2}FeO_{3-\delta}$. P_{O2} is the oxygen partial pressure. $Fe^{'}_{Fe}$, $Fe^{\times}_{Fe}$ and $Fe^{\bullet}_{Fe}$ represents an Fe cation at the Fe site in the oxidation state of Fe^{II}, Fe^{III} and Fe^{IV}, respectively. The relationship of the $La_{0.8}Sr_{0.2}FeO_{3-\delta}$ oxygen deficiency (δ) with the steam conversion at 930 °C is given in Figure S5, by using the equilibrium constants reported by Mizusaki et al.[6]. The reduction of Fe^{IV} conversion to Fe^{III} and Fe^{III} to Fe^{II} occur in two separated stages $0 < \delta < 0.1$ and $0.1 < \delta < 0.6$. At the steam conversion of 62.3%, which is the thermodynamically maximum steam conversion for FeO_x-H_2O-H_2 ternary system, the δ is equal to approximately 0.107. When $\delta > 0.14$, steam conversion of the defected perovskite is greater than 99%. This contributes to the high steam conversion obtained by the LSF supported iron oxide.

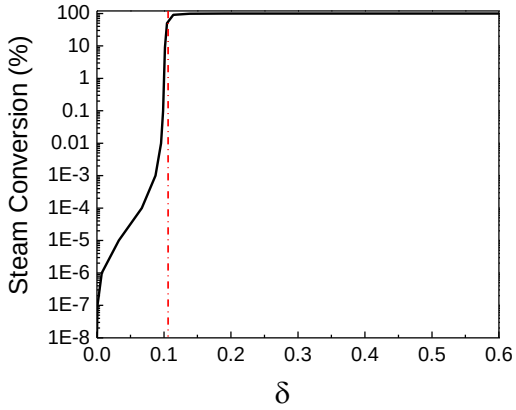

Figure S5: relationship between $La_{0.8}Sr_{0.2}FeO_{3-\delta}$ oxygen deficiency (δ) and steam conversion at 930 °C. Red dash-dotted line displays thermodynamically predicted steam conversion for Fe→FeO phase transition

Pure LSF tested in the TGA with H_2 reduction (Figure S6) shows a total of ~10.5% weight loss. A comparison of the weight gain during steam oxidation from TGA results and defect model calculation are shown in Table S3. The weight gain under different steam conversion is normalized by fully oxidized sample weight. The data predicted by the defect model shows good consistency with experimental results. Based on the experimental results and theoretical calculations, LSF could achieve a higher steam conversion than iron oxides. Therefore, LSF is partially oxidized before reduced metallic iron start to react with steam.

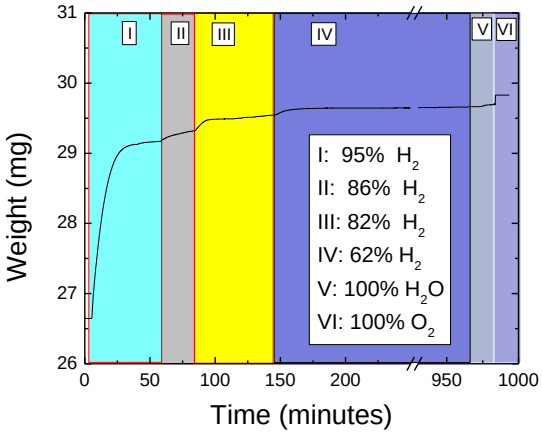

Figure S6: Pure LSF particle TGA test with steam and hydrogen mixture oxidation at 930°C

Table S3: Comparison on the normalized weight gain in the steam oxidation of the TGA results and defect model calculation

	Defect Model Calculation	Experimental Data
>95% conversion	10.0%	8.5%
>86% conversion	10.2%	9.0%
>62% conversion	10.2%	10.1%

The theoretical steam to H_2 conversion based on the defect model can be calculated under two idealized cases:

(i) Additive effect of iron oxide and LSF

Under the additive scenario, iron (oxides) and LSF are well mixed and act independently for steam conversion in a simultaneous manner. Assuming that iron (oxide) is the limiting reactant, parallel reactions will lead to the following conversion:

$$X_{H_2O} = \frac{n_{H_2O_{converted}}}{n_{H_2O_{initial}}} = \frac{n_{O-LSF} + n_{O-Fe}}{\frac{n_{O-LSF}}{X_{H_2O-LSF}} + \frac{n_{O-Fe}}{X_{H_2O-Fe}}} \qquad \text{Equation S11}$$

(ii) Sequential effect of iron oxide (first) and LSF (second)

Under the sequential scenario, iron (oxides) and LSF are assumed to react with steam in a consecutive manner. In such a configuration, defect in reduced LSF will be able to further enhance steam conversion by reacting with the steam-hydrogen mixture resulted from steam-iron reaction. Assuming that iron (oxide) is the limiting reactant, sequential reactions will lead to the following conversion:

$$X_{H_2O} = \frac{n_{H_2O_{converted}}}{n_{H_2O_{initial}}} = \frac{n_{O-LSF} + n_{O-Fe}}{\frac{n_{O-Fe}}{X_{H_2O-Fe}}} \qquad (n_{O-LSF} < n_{O-Fe}(\frac{1}{X_{H_2O-Fe}} - 1)) \qquad \text{Equation S12}$$

$n_{O\text{-}Fe}$ and $n_{O\text{-}LSF}$ are the mole of oxygen gain in the water splitting reaction, and $X_{O\text{-}Fe}$ and $X_{O\text{-}LSF}$ are the corresponding steam conversion. The calculated results are shown in Figures 2 and 3 in the main paper.

Steam to H_2 conversion in the fixed bed experiments

In order to demonstrate the high steam conversion, iron oxides with 25% and 40% $La_{0.8}Sr_{0.2}FeO_{3-\delta}$ support and reference Fe_3O_4-$MgAl_2O_4$ are tested in a fixed-bed reactor. Hydrogen is selected as the fuel in the reduction step for accurate initial assessment of steam conversion in the water-splitting step since no side reactions are likely to take place between hydrogen and the redox catalyst samples. The redox catalyst is reduced by H_2 for 30 minutes in the first step. After reduction, 6.8 ml min^{-1} steam with 15 ml min^{-1} N_2 is injected from the bottom of the reactor to oxidize the redox catalysts for 40 minutes. Then alternate reduction and regeneration of the redox catalyst will be implemented by the same procedure. The XRD pattern (Figure S7) indicates that redox catalyst is fully reduced to metallic iron in the reduction step. And in the oxidation step, it is regenerated into a mixture of Fe, FeO and Fe_3O_4, which has an average composition of $FeO_{0.5}$ by mass balance.

The impact of temperature on the steam to H_2 conversion is illustrated in Figure S8A for Fe_3O_4-LSF (40wt% LSF). There are two competing effects: (i) increasing temperature leads to lower steam conversion based on thermodynamics; (ii) increasing temperature enhances the reaction kinetics and hence increases steam conversion in the fixed bed. At a fixed space velocity of approximately 6 $minutes^{-1}$, the maximum steam to H_2 conversion of Fe_3O_4-LSF(40wt%) is archived at 930 °C, which is consistent with the results of Fe_3O_4-LSF(25wt%). Therefore, 930 °C is selected as the nominal temperature in the paper. After that, multi-cycle experiment is

conducted at 930 °C in the fixed bed. As shown in Figure S8B, the average steam to H_2 conversion over 12 cycles of Fe_3O_4-LSF (25wt% LSF) and Fe_3O_4-LSF (40wt% LSF) is 64.0% (±0.67%) and 67.1% (±1.27%) with 95% confidence, respectively. In comparison, $MgAl_2O_4$ spinel supported iron oxide shows a steam conversion of 39%, which is 25-28% lower than LSF promoted Fe_3O_4 particle.

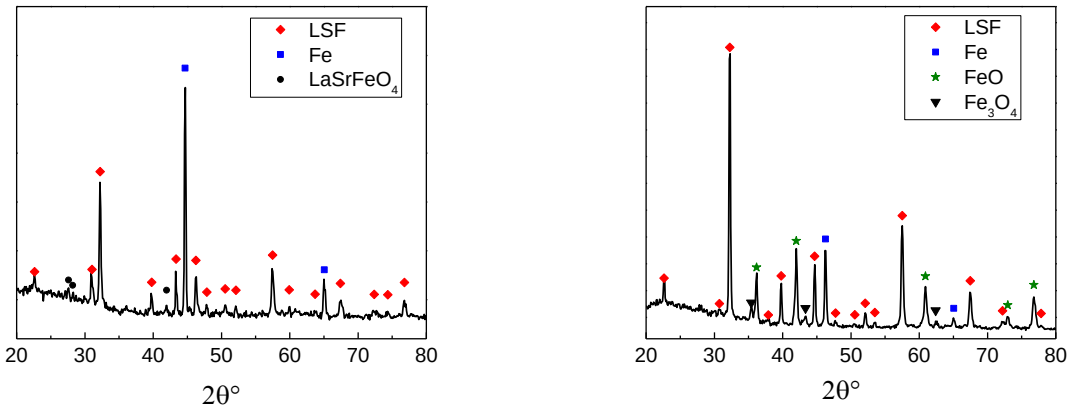

Figure S7: XRD Pattern of Fe_3O_4-LSF redox catalyst in the fixed bed experiment at 930 °C (A) reduced by hydrogen and (B) regenerated by steam.

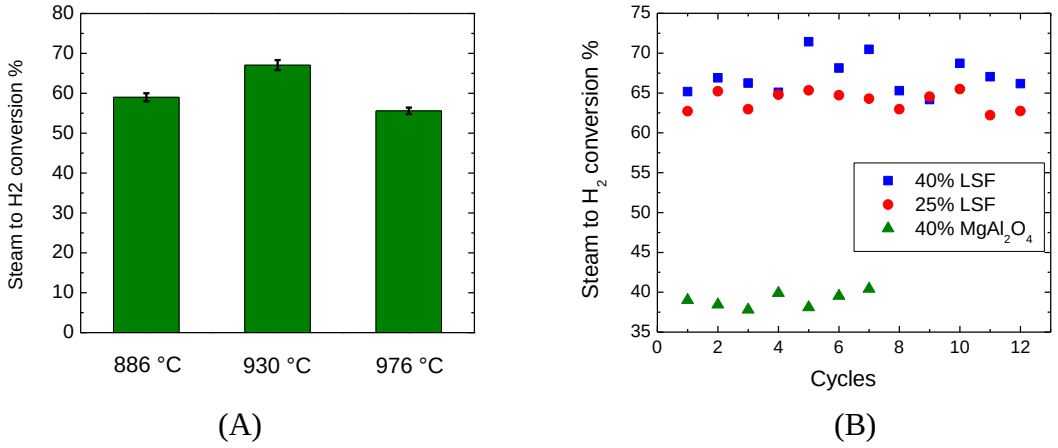

Figure S8: (A) The temperature effects on the steam to H_2 conversion per cycle for Fe_3O_4-LSF (40wt% LSF). (B) Average steam to H_2 conversion per cycle over multi-cycle at 930 °C.

Methane oxidation reaction in the layered reverse-flow reactor

Redox study on Fe_3O_4-LSF is conducted in a layered reverse-flow reactor, where methane is injected from the top of the bed to reduce the redox catalyst. Neal et al. [7] reported that LSF has higher resistance towards coke formation compared to the iron oxides. In order to inhibit excessive carbon formation from methane decomposition, methane injection is stopped when $H_2/(CO+CO_2)$ molar ratio exceeds 2. The product gas concentration as a function of time in the reducer is shown in Figure S9. The average methane conversion under the fixed-bed mode is

above 99%. The corresponding syngas ($CO+H_2$) yield is ~62% (±3%) with a H_2/CO molar ratio of ~2.2 (±0.1).

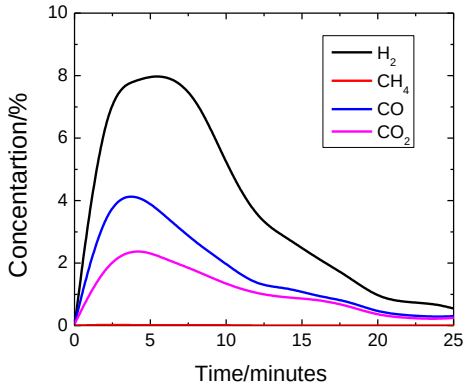

Figure S9: Product gases concentration (N_2 and H_2O-free basis) as a function of time in methane oxidation step.

Water-splitting reaction in the layered reverse-flow reactor

Water-splitting or steam-iron reaction is initiated by introducing steam into the reactor after the methane conversion step. Figure S10 shows a representative H_2 purity profile (water-free and N_2-free basis) as a function of time. At the beginning of the steam oxidation, small amounts of CO and CO_2 are detected, which corresponds to the gasification of carbon deposited in the methane oxidation step. Since it is well controlled to minimize the coke formation, an overall H_2 purity of 98.5% is achieved in the water-splitting step.

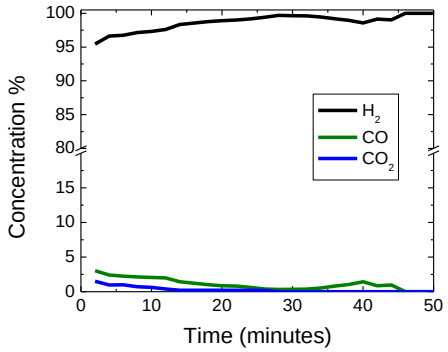

Figure S10: H_2 concentration (water-free) during the water splitting step as a function of time at 930 °C after the reduction step.

The layered reverse-flow reactor concept is proved in fixed bed experiments. Figure S11 shows a comparison of real time steam conversion between with and without layered reverse-flow. In the layered reverse-flow experiment, steam is going through the bottom Fe_3O_4-LSF bed with ~64.0% steam converted in the first place. And then the top layer of reduced LSF further converts part of

the remaining steam into H_2, resulting in exceptional overall steam conversion of 77.2%. The average steam to H_2 conversion in the layered reverse-flow experiment is ~10% high than the one without reverse flow.

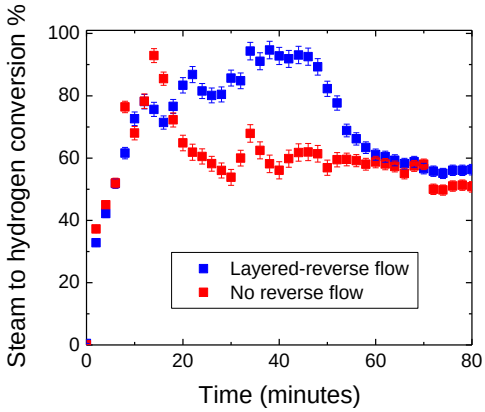

Figure S11: Real time steam conversion in oxidation with and without layered reverse-flow

Process modeling of the hybrid solar-redox scheme

In the hybrid solar-redox scheme (Figure S12A), liquid fuel and hydrogen are produced from methane and integrated solar energy in two redox steps.[8,9] In the first step (reducer), methane is partial oxidized by redox catalyst material (Fe_3O_4-LSF) into CO and H_2, which is then converted into naphtha and diesel in the Fischer-Tropsch (F-T) reactors. In the subsequent step (oxidizer), steam oxidizes the reduced redox catalyst material from the previous step, producing concentrated H_2. ASPEN Plus simulation (Figure S12B) is used to estimate reactor and process performances of the hybrid solar-redox concept. Detailed simulation assumptions with respect to materials, simulation modules, property methods, physical property databanks, and key operating parameters are summarized in our previous publication.[8] The temperature of the reducer and oxidizer is set at 930 °C, which matches the experimental conditions. Two simulation cases with different steam to hydrogen conversions in the oxidizer are simulated, and the results are shown in Table S4. Case I is using the steam conversion of 77.2% which is achieved from the proposed layered reverse-flow reactor. Case II assumes steam conversion of 20%, which is the maximum reported conversion from literature. The incremental heat requirement from the low steam conversion in Case II is provided by conventional methane combustion, so that the solar energy usage is identical in the two cases. All other simulation assumptions and parameters are assumed to be same.[8] Under the scenario of no CO_2 capture, case II uses 48% more methane to compensate the increased heat requirement through combustion. Therefore, with the benefit of exceptional steam to H_2 conversion, Case I has the overall process thermal efficiency of 63.1%(HHV), which is 15.1% higher than case II with lower steam conversion.

A life cycle greenhouse gas (GHG) footprint analysis is conducted, which considers the contributions from natural gas upstream and energy conversion facility. The estimated upstream natural gas emission based on US-DOE report is in the range of 6.1-9.1 g CO_2/MJ for various feedstocks.[10] The emission analysis from energy conversion facility is based on ASPEN model results. When calculating the emission on hydrogen, a CO_2 emission quota for the liquid fuel products is subtracted. The emission on liquid fuel products from the solar-redox process is

assumed to be are identical to the one of petroleum derived fuels, which is reported at 90 g CO_2/ MJ[11]. Two scenarios are investigated for cases with and without CO_2 capture. 0.75 MJ/kg CO_2 energy consumption is assumed for the amine-based CO_2 capture.[2] The CO_2 footprint from the hybrid solar-redox scheme are shown in Table S3.

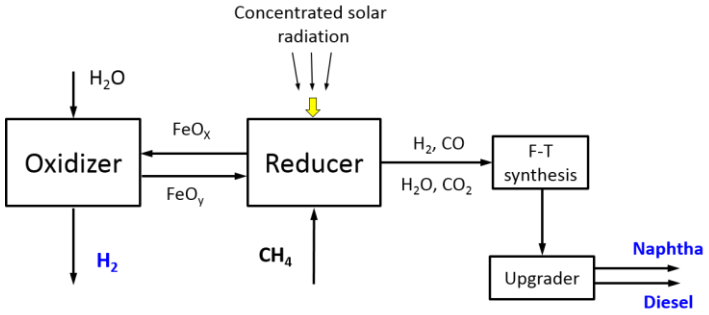

(A)

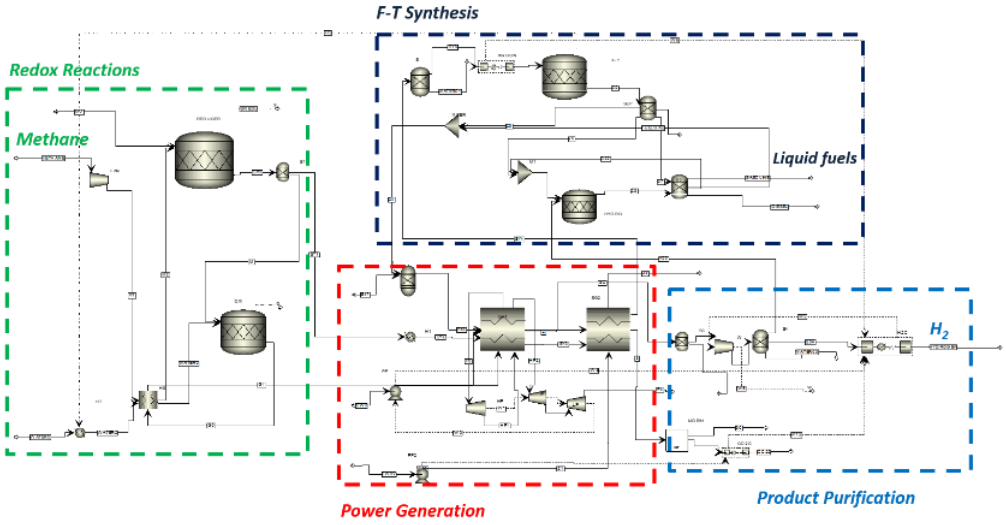

(B)

Figure S12: (A) Simplified schematic and (B) ASPEN flowsheet of the hybrid solar-redox scheme

Table S3. Process simulation results on the hybrid solar-redox cases

		Case I		**Case II**	
		Without CO_2 Capture	With CO_2 Capture	Without CO_2 Capture	With CO_2 Capture
Steam to H_2 conversion	%	77.2%		20%	
Methane input	t hr^{-1}	8.0		11.9	
Overall process efficiency	HHV%	63.1	61.3	48.0	45.4
CO_2 footprint on all hydrogen	g CO_2/MJ H_2	44.4	9.0	96.7	29.0
CO_2 footprint on all product	g CO_2/MJ	65.5	38.8	97.3	45.7

References:

1. N. L. Galinsky, Y. Huang, A. Shafiefarhood and F. Li, *ACS Sustain. Chem. Eng.*, 2013, **1**, 364–373.
2. G. Rochelle, E. Chen, S. Freeman, D. Van Wagener, Q. Xu and A. Voice, *Chem. Eng. J.*, 2011, **171**, 725–733.
3. G. T. Rochelle, *Science*, 2009, **325**, 1652–1654.
4. D. R. Gaskell, *Introduction to metallurgical thermodynamics*, Hemisphere Pub. Corp., 1981.
5. A. Murugan, A. Thursfield and I. S. Metcalfe, *Energy Environ. Sci.*, 2011, **4**, 4639–4649.
6. J. Mizusaki, M. Yoshihiro, S. Yamauchi and K. Fueki, *J. Solid State Chem.*, 1985, **58**, 257–266.
7. L. M. Neal, A. Shafiefarhood and F. Li, *ACS Catal.*, 2014, **10**, 3560–3569.
8. F. He, J. Trainham, G. Parsons, J. S. Newman and F. Li, *Energy Environ. Sci.*, 2014, **7**, 2033–2042.
9. F. He and F. Li, *Int. J. Hydrog. Energy*, 2014, **39**, 18092–18102.
10. T. Skone, 2014, US DOE/NETL-2014/1646. http://www.netl.doe.gov/File%20Library/Research/Energy%20Analysis/Life%20Cycle%20Analysis/NETL-NG-Power-LCA-29May2014.pdf
11. K. Gerdes, T. Skone, 2009, US DOE/NET. http://www.netl.doe.gov/File%20Library/Research/Energy%20Analysis/Publications/CompTranspFuels-GHGEmisEnergySecImpacts---Pres.pdf